Strong-Field Atomic Phase Matching

Carlos Trallero-Herrero,[1] J. L. Cohen,[2] and Thomas Weinacht[1]

[1]*Department of Physics, Stony Brook University, Stony Brook, New York 11794, USA*

[2]*FOCUS Center, Department of Physics, University of Michigan, Ann Arbor, Michigan 48103, USA*

(Received 22 September 2005; revised manuscript received 11 January 2006; published 16 February 2006)

We interpret a learning-control experiment with the goal of optimizing multiphoton population transfer in atomic sodium in the strong-field limit. Despite multiple experimental constraints, a learning algorithm discovers optimal pulses that can be understood in terms of a simple dynamic picture of the atom-field interaction. We show that the shaped pulses counteract the dynamic Stark-induced stimulated emission that would otherwise impede the efficient use of a π pulse to invert a multiphoton transition.

DOI: 10.1103/PhysRevLett.96.063603 PACS numbers: 42.50.Hz

Controlling atomic and molecular dynamics with strong laser fields has generated significant interest in recent years. Experiments have demonstrated coherent control over a wide variety of atomic and molecular systems using shaped ultrafast laser pulses [1–11]. In many cases, particularly when using strong fields where the interaction is highly nonperturbative, it is difficult to predict optimal control fields *a priori*. As a result, learning algorithms have been used to discover optimal fields for control [12]. While learning algorithms have been successful in discovering optimal control fields, it is generally difficult to understand the physical mechanisms underlying control. Here, we consider a simple atomic system in the nonperturbative limit [13,14]. Strong-field control of the atom-field dynamics can counteract the deleterious effect of the dynamic Stark effect, which otherwise prevents efficient population of a target state [15]. The learning algorithm discovers optimal excitation pulses that are consistent with a simple and intuitive picture of the dynamics during control of a two-photon absorption process in atomic Na, where the control field ''phase matches'' the coupled atom-field system to optimize excitation of the targeted atomic transition.

One approach to understanding strong-field dynamics has been to take weak-field solutions [9,10,16] and adapt them to the strong-field limit. This approach has been used to take a large class of weak-field solutions for selective multiphoton population transfer to the strong-field limit [17]. The result is an understanding of how to maintain selectivity but not efficiency (i.e., population inversion). Here, we demonstrate a learning-control experiment that discovers pulse shapes which are very efficient for transferring population in the face of strong dynamic Stark shifts. The atom-field interaction in strong fields is essentially different from that in weak fields because in the strong-field regime the resonance condition is dynamic, whereas in the weak field it is static. This means that a simple frequency domain interpretation [10,16] cannot account for the changing resonance condition found in strong-field excitation. This is highlighted by the fact that the optimal pulse for weak-field multiphoton excitation (an unshaped laser pulse in the absence of intermediate resonances) performs arbitrarily poorly in strong fields [15].

An important aspect of any closed-loop learning-control experiment is the effect that constraints have on the solutions [18]. The solutions are constrained in many important ways in our experiments. There is a fixed pulse energy, bandwidth, and pulse shaper resolution. These constraints preclude the learning algorithm [a genetic algorithm (GA) in our experiment [19]] from finding the simple and intuitive solution in which the laser frequency follows the instantaneous energy separation of the two states [15]. However, the GA finds solutions that greatly improve upon an unshaped pulse and can efficiently excite the atoms. Furthermore, using the understanding developed in [15], we show how these constrained solutions can be understood in terms of a strong-field atom-field phase matching picture. This picture, which explicitly considers the dynamic resonance resulting from the dynamic Stark shift, should be helpful for interpreting molecular learning-control experiments, where resonances evolve in time as a result of nuclear motion.

The goal of our learning-control experiments was to optimize population transfer from the $3s$ to the $4s$ state in atomic Na, which is two-photon resonant at 777 nm. Previous work on Na [20,21] looked at multiphoton ionization as a function of laser intensity and the delay between two pulses. Modulations in the ionization yield as a function of laser intensity highlighted the importance of dynamic Stark shifts, and control over ionization via pump-probe delay for two pulses was shown to give significant improvement in the ionization rate over a single, unshaped laser pulse. The improvement in the ionization yield for two pulses over a single pulse was shown to be a result of coherences between states in a ladder system consisting of the $3s$, $4s$, and $7p$ states. Our control goal is to maximize population transfer between two bound states rather than ionizing through a ladder of states. We target a specific quantum state that is evolving in a strong field on a femtosecond time scale.

Our experiments make use of a Ti:Sapphire laser system that produces 30 fs pulses with an energy $\approx$1 mJ at a

repetition rate of 1 KHz. The laser is tunable from 772 to 784 nm. The amplified pulses from our laser system are shaped in an acousto-optic modulator based pulse shaper (AOM PS) [22]. In order to generate fields strong enough to invert the $3s$-$4s$ transition in our atomic sample, we need to focus the laser pulses. However, it is critical for the interpretation of the results that the measurement does not average over atoms which are exposed to very different laser intensities. As the dynamic Stark shift is proportional to the laser intensity, atoms that see different peak intensities require different pulse shapes to optimize excitation. Thus, we produce a laser focus with minimal intensity variation by imaging a spatially filtered focus into the heat pipe oven sample chamber as shown in Fig. 1(a). Modest pulse energies (less than 20 μJ) and a long focal length lens (1 m) used to focus the beam into the pinhole allow us to avoid nonlinear processes such as continuum generation. Pulse measurements before and after the pinhole indicate that the pulse shape does not change in passing through the pinhole. The spatial filtering reduces the transverse intensity variation in the focus to about 20%. We also measure florescence from a short enough longitudinal region of the focus such that intensity variations along the beam propagation direction are negligible. The reduction of spatial averaging allows the learning algorithm to control a more uniform atomic ensemble, allowing us to focus on the single atom response rather than averaging over atoms exposed to a large range of intensities.

Fluorescence light from the center of the heat pipe was collected at 90° with respect to the beam propagation direction with an $f2$ lens and imaged onto a photomultiplier tube (PMT). An interference filter centered at 589 nm was used to isolate light from the $3p$-$3s$ transition, populated primarily by spontaneous decay from the $4s$ state to the $3p$ state. The signal from the PMT was sent to a computer and processed by a GA that controls the pulse shaper in a feedback loop. Details of our learning algorithm can be found in [19]. By averaging the fluorescence from 30 laser shots for each pulse shape, we were able to limit the noise to less than 1% of the signal. In order to ensure that we were working in the strong-field limit, we measured the fluorescence yield as a function of laser pulse energy for an unshaped 35 fs laser pulse. With the spatial filtering in place as described above, the yield showed evidence of Rabi oscillations. Without the spatial filtering, the yield increased roughly linearly with intensity as far as we could increase the laser intensity, which was far above the intensity required for a two-photon π pulse. Having a constant intensity in the interaction region thus proves extremely important for efficient control in the strong-field limit.

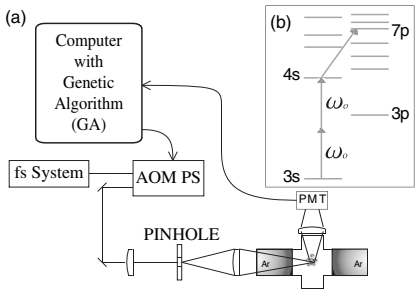

FIG. 1. (a) Experimental setup. (b) Sodium energy level diagram.

While our pulse shaper is capable of shaping both the spectral phase and amplitude of the pulses, we limited the pulse shaping in this experiment to phase only in order to work at a fixed pulse energy and to keep the number of degrees of freedom low enough for proper convergence of the learning algorithm. We performed the learning-control experiments at three different central wavelengths (772, 777, and 784 nm) around the bare resonance (777 nm), because detuning plays an important role in the physics underlying control. For all three detunings, the GA was able to find pulse shapes that outperformed an unshaped pulse. At 777 and 784 nm, an optimal pulse increased the fluorescence yield by factors of 4.5 and 5 over an unshaped pulse, respectively. To the blue, the increases were more modest—around a factor of 2.5. Running the GA in the weak-field regime, where the pulse area was much less than π, yielded no improvement relative to an unshaped laser pulse.

In the weak-field regime with no intermediate resonances, an unshaped pulse is optimal for maximizing multiphoton population transfer [9,10]. However, in the strong-field regime, a shaped pulse can do better. This is a direct consequence of the dynamic Stark shift, which makes the population transfer for an unshaped pulse quite inefficient [15]. It is not surprising that the improvements are larger for red and zero detuning, because an unshaped, blue-detuned pulse can roughly compensate for the average dynamic Stark shift, resulting in more efficient population transfer than an unshaped pulse with zero detuning.

Optimal pulse shapes discovered by the algorithm were measured using second harmonic generation frequency resolved optical gating. The pulses had sufficient energy for a π pulse, with peak unshaped pulse intensities of about 3×10^{11} W/cm^2. The GA found an array of optimal pulses for each detuning. While we have analyzed many of the solutions, here we interpret a representative solution for each central frequency, showing how the solutions at each detuning are consistent with strong-field atom-field phase matching. Figures 2(a)–2(c) show optimal pulse shapes for central wavelengths of $\lambda_0 = 784$, 772, and 777 nm, respectively.

For red detuning, the GA found the most consistent set of solutions, which have as a common feature the presence of two peaks separated in time, with a slowly and smoothly varying temporal phase. When the laser was tuned to the blue at $\lambda_0 = 772$ nm, the GA found an array of solutions, which varied from complicated intensity and phase structure to a simple single pulse with a slowly varying temporal phase. Finally, at $\lambda_0 = 777$ nm, various solutions con-

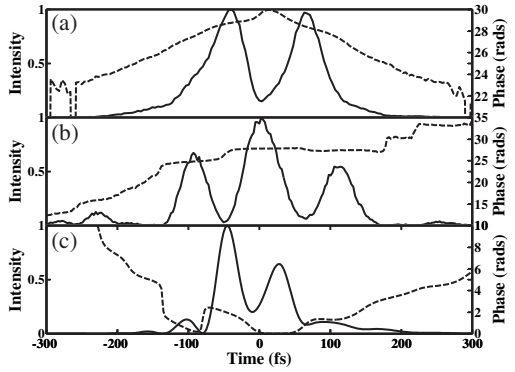

FIG. 2. Optimal pulses found by the GA for transferring population at (a) $\lambda_0 = 784$ nm, (b) $\lambda_0 = 772$ nm, and (c) $\lambda_0 = 777$ nm.

sisted mostly of two and three subpulses. A more detailed, principle control analysis [23] of the full solution set is underway and is the subject of a future publication. The different solutions for the three detunings do not immediately suggest a particular mechanism. However, calculations of the atom-field interaction reveal that all three solutions can be understood in terms of a very simple and intuitive phase matching picture. We performed numerical integrations of the Schrödinger equation in the rotating wave approximation after adiabatically eliminating the nonresonant atomic levels. These calculations are detailed in a previous publication [15]. Here we only summarize them briefly. In a frame that rotates at twice the laser frequency ω_0, the atom-field Hamiltonian is

$$\hat{\mathbf{H}} = \begin{pmatrix} -\frac{1}{2}[\delta_\omega^{(s)}(t) - \Delta + \dot{\varphi}(t)] & \chi^*(t) \\ \chi(t) & \frac{1}{2}[\delta_\omega^{(s)}(t) - \Delta + \dot{\varphi}(t)] \end{pmatrix}. \tag{1}$$

$\chi(t)$ is the two-photon Rabi frequency, $\delta_\omega^{(s)}(t)$ is the differential Stark shift between the ground and excited states, and $\varphi(t)$ represents the phase of the laser pulse. While the $7p$ state, which is nearly resonant with the $4s$ state, is not included in the Hamiltonian above for simplicity, it was included in all of our calculations. Our calculations indicate that while the inclusion of the $7p$ state is important for quantitative agreement between theory and experiment (particularly at 777 nm), it is possible to understand the optimal solutions without it.

The calculations aim to determine whether we can understand the optimal pulse shapes discovered by the GA in terms of a strong-field atom-field phase matching picture. The most salient feature of the optimal pulses for red detuning ($\lambda_0 = 784$ nm) is the double pulse structure, with a slowly varying temporal phase. We therefore examined the population transfer numerically as a function of delay and detuning for a pair of pulses. Figure 3(a) shows the final $4s$ population for a pair of pulses as a function of detuning from the bare resonance and the time delay between the two pulses. The intensity is chosen such that the integral of $2\chi(t)$ is π for the pulse pair (minimum pulse energy required for full inversion) and the duration of each pulse is $\tau = 50$ fs. From the figure we can see that two pulses can be more effective than one for proper choice of detuning and delay. The optimal pulse separation for $\lambda_0 = 784$ nm is about 110 fs, which matches the separation between peaks in the experimental solution [see Fig. 2(a)]. The atom-field interaction leading to the results shown in Fig. 3(a) can be understood with the help of Figs. 4(a) and 4(d) [which consider pulse shapes corresponding to the x mark in Fig. 3(a)]. Panel (a) shows the $4s$ population as a function of time for unshaped and optimally shaped pulses, and panel (d) shows the atom-field phase, $\alpha(t)$. $\alpha(t)$ is given by the integral of the diagonal terms in the two level atom-field Hamiltonian [15]:

$$\alpha(t) = \int_{-\infty}^{t} \delta_\omega^{(s)}(t')dt' - \Delta t + \varphi(t). \tag{2}$$

Panel (a) (Fig. 4) shows that for a single unshaped laser pulse the population in the $4s$ state goes up and comes back down to nearly zero during the pulse. For the optimal pulse solution, the population is as close as possible to being monotonically increasing for that detuning. If the atom-field phase goes beyond $\pm\pi/2$ during the pulse, the pulse begins to stimulate emission rather than absorption, leading to less efficient population transfer. This is why it is more efficient to split the pulse into two such that $\alpha(t)$ evolves slower and the atom can rephase with the field between subpulses [as shown in panel (d)], minimizing the amount of stimulated emission. Note that $\alpha(t)$ evolves by 2π between pulses in Fig. 4(d). The action of turning off the nonlinear coupling between states while the atom and field rephase is analogous to quasiphase matching in nonlinear optics [24]. The separation of the excitation energy into two temporal pulses allows full use of the π pulse while the single-peaked π pulse imposes a Stark shift that forces a rapid phase-mismatch between the atom and effective two-photon field amplitude [15]. Of course, tuning the central frequency of the laser pulse would also provide a valid solution, but this is prevented by the common experimental constraint of a fixed central frequency.

A quantitative formulation of the phase matching picture is that maximization of the upper state population entails

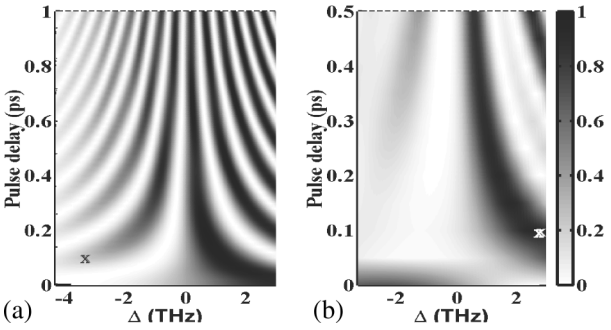

FIG. 3. (a) Final $4s$ population after interacting with a pair of laser pulses as a function of pulse delay and detuning. (b) Final $4s$ population after interacting with three pulses as function of pulse delay for pulses with a $\pi/2$ phase jump between pulses.

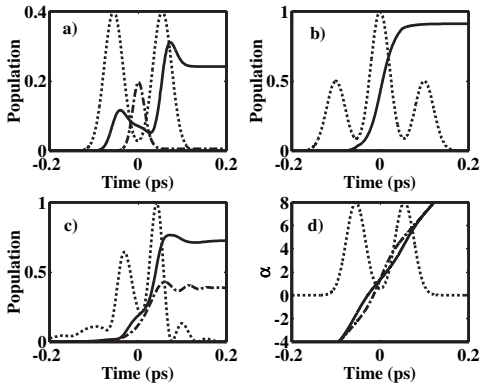

FIG. 4. Panels (a), (b), and (c) show the $4s$ population for shaped (solid line) and unshaped pulses (dash-dotted line) vs time for central wavelengths of $\lambda_0 = 784$ nm, $\lambda_0 = 772$ nm, $\lambda_0 = 777$ nm, respectively. Panels (a) and (b) are for parametrized pulse shapes, and panel (c) is for a measured pulse. Panel (d) shows the atom-field phase $\alpha(t)$ for an unshaped pulse (dash-dotted line) and the optimal pulse shown in panel (a) (solid line). All panels also show the shaped pulse intensity profiles (dotted line).

maximizing the absolute value of the integral:

$$\int_{-\infty}^{\infty} \chi(t) \exp[i\alpha(t)]dt \tag{3}$$

for a fixed area pulse, such that $\int_{-\infty}^{\infty} \chi(t)dt = \frac{\pi}{2}$. The value of the integral in Eq. (3) increases by a factor of more than 6 for the optimal two pulse solution in Figs. 2(c) and 4(c) compared with an unshaped pulse. As the solution for 772 nm shown in Fig. 2(b) exhibits three pulses with phase jumps between pulses, we examine the population transfer as a function of time delay for three pulses with $\pi/2$ relative phase jump between pulses. Figures 3(b) and 4(b) show the simulation results for such field. The pulse in Fig. 4(b) corresponds to the x mark in Fig. 3(b). From the density plot, we can see that three pulses separated by 100 fs [such as the solution displayed in Fig. 2(b)], with $\pi/2$ phase jumps between pulses leads to optimal excitation. The value of the integral in Eq. (3) is also maximized for such a pulse.

In order to interpret the solutions at 777 nm, which were more difficult to parametrize because of their more complicated structure, we integrated the Schrödinger equation numerically for the algorithm-generated experimental pulse shapes and also calculated the integral in Eq. (3). In Fig. 4(c), we show the $3s$ and $4s$ populations as function of time for the experimental pulse of Fig. 2(c), as well as for an unshaped pulse. The increases in the population transfer are comparable to the increases in the integral in Eq. (3) for the optimal pulse over an unshaped pulse. Small phase errors in our pulse measurement and uncertainties in the experimental laser intensity account for the difference between the experimental and calculated contrast between a shaped and an unshaped laser pulse.

In weak fields, with no near resonant states between the two states of interest, there is no solution that can outperform an unshaped laser pulse. However, in strong fields, the dynamic Stark shift pushes the two states apart, increasing the instantaneous energy difference, and therefore leading to a phase advance of the atom with respect to the field. This phase advance can cause the atom to become out of phase with the driving field, resulting in stimulated emission rather than absorption. Ideally, if the laser frequency could follow the instantaneous energy difference in the atom, then the atom-field phase would not slip and population transfer would be maximized [15]. As the GA cannot change the spectrum of the laser pulse, this solution is not allowed and the best that the GA can do is to vary α and $I(t)$ such that the integral in Eq. (3) is maximized. The experiments show that it can do this to achieve the maximum population transfer possible at each detuning.

In conclusion, we have used a learning algorithm to discover strong-field laser pulses that are more efficient than an unshaped pulse in driving two-photon absorption. The solutions found by the GA can be understood in terms of atom-field phase matching in the presence of a strong optical field. The results are promising for understanding closed-loop learning-control experiments in general.

This research is supported by the National Science Foundation under Grant No. 0244748.

[1] Z. Amitay *et al.*, Chem. Phys. **267**, 141 (2001).
[2] A. Assion *et al.*, Science **282**, 919 (1998).
[3] C. Bardeen *et al.*, Chem. Phys. Lett. **280**, 151 (1997).
[4] R. Bartels *et al.*, Nature (London) **406**, 164 (2000).
[5] C. Daniel *et al.*, Science **299**, 536 (2003).
[6] M. Dantus, Annu. Rev. Phys. Chem. **52**, 639 (2001).
[7] J. Herek *et al.*, Nature (London) **417**, 533 (2002).
[8] R. Levis, G. Menkir, and H. Rabitz, Science **292**, 709 (2001).
[9] D. Meshulach and Y. Silberberg, Nature (London) **396**, 239 (1998).
[10] D. Meshulach and Y. Silberberg, Phys. Rev. A **60**, 1287 (1999).
[11] T. Weinacht, J. Ahn, and P. Bucksbaum, Nature (London) **397**, 233 (1999).
[12] R. Judson and H. Rabitz, Phys. Rev. Lett. **68**, 1500 (1992).
[13] C. W. S. Conover *et al.*, Phys. Rev. A **65**, 033414 (2002).
[14] L. Sirko, S. A. Zelazny, and P. M. Koch, Phys. Rev. Lett. **87**, 043002 (2001).
[15] C. Trallero-Herrero *et al.*, Phys. Rev. A **71**, 013423 (2005).
[16] A. Prakelt *et al.*, Phys. Rev. A **70**, 063407 (2004).
[17] N. Dudovich *et al.*, Phys. Rev. Lett. **94**, 083002 (2005).
[18] H. Rabitz, Science **299**, 525 (2003).
[19] F. Langhojer *et al.*, J. Chem. Phys. **122**, 014102 (2005).
[20] R. Jones, Phys. Rev. Lett. **74**, 1091 (1995).
[21] R. Jones, Phys. Rev. Lett. **75**, 1491 (1995).
[22] P. Tian *et al.*, Science **300**, 1553 (2003).
[23] J. L. White, B. Pearson, and P. H. Bucksbaum, J. Phys. B **37**, L399 (2004).
[24] A. Paul *et al.*, Nature (London) **421**, 51 (2003).